STARS

University of Central Florida
STARS

Faculty Bibliography 2010s

Faculty Bibliography

1-1-2013

Mobility transition from ballistic to diffusive transport in non-Hermitian lattices

T. Eichelkraut

R. Heilmann

S. Weimann

Simon Stützer

Felix Dreisow

See next page for additional authors

Find similar works at: https://stars.library.ucf.edu/facultybib2010
University of Central Florida Libraries http://library.ucf.edu

Recommended Citation

University of Central Florida

STARS
Showcase of Text, Archives, Research & Scholarship

Authors

T. Eichelkraut, R. Heilmann, S. Weimann, Simon Stützer, Felix Dreisow, Demetrios N. Christodoulides, Stefan Nolte, and Alexander Szameit

Mobility transition from ballistic to diffusive transport in non-Hermitian lattices

T. Eichelkraut[1], R. Heilmann[1], S. Weimann[1], S. Stützer[1], F. Dreisow[1], D.N. Christodoulides[2], S. Nolte[1] & A. Szameit[1]

Within all physical disciplines, it is accepted that wave transport is predetermined by the existence of disorder. In this vein, it is known that ballistic transport is possible only when a structure is ordered, and that disorder is crucial for diffusion or (Anderson-)localization to occur. As this commonly accepted picture is based on the very foundations of quantum mechanics where Hermiticity of the Hamiltonian is naturally assumed, the question arises whether these concepts of transport hold true within the more general context of non-Hermitian systems. Here we demonstrate theoretically and experimentally that in ordered time-independent $\mathcal{PT}$-symmetric systems, which are symmetric under space-time reflection, wave transport can undergo a sudden change from ballistic to diffusive after a specific point in time. This transition as well as the diffusive transport in general is impossible in Hermitian systems in the absence of disorder. In contrast, we find that this transition depends only on the degree of dissipation.

[1] Institute of Applied Physics, Friedrich-Schiller-Universität Jena, Max-Wien-Platz 1, 07743 Jena, Germany. [2] CREOL, The College of Optics and Photonics, University of Central Florida, Orlando, Florida 32816, USA. Correspondence and requests for materials should be addressed to A.S. (email: alexander.szameit@uni-jena.de).

The deceleration of wave transport in a lattice due to disorder was introduced in physics about 100 years ago with the famous Drude model. Paul Drude explained the conductance of metals by free electrons that are scattered by the atomic lattice, which in turn results in a diffusive transport[1]. The diffusion process is ubiquitous. It governs the effects of electric and thermal conductivity in solids[1,2], particle mixing in fluids[3] and spin diffusion effects[4], just to name a few. In this context, it is generally agreed that all systems that exhibit sub-ballistic transport are inherently disordered. Today, disorder is explored in many disciplines, such as optics[5], solid-state physics[6], acoustics[7] and matter waves[8,9]. In particular, optical systems attracted much interest, and so far numerous sub-ballistic transport phenomena based on disorder have been observed; these include the Anderson localization[5,10,11], quantum decoherence[12], Levy flights[13] and anomalous diffusion[14].

The understanding of diffusive (and in general sub-ballistic) transport naturally assumes Hermiticity of the Hamiltonian, as this ensures the reality of the eigenvalue spectrum and, therefore, energy conservation. However, dissipative (that is, lossy) systems that interact with their environment are by far the most common. With the damped pendulum as the simplest example, dissipation is the basis for phenomena like the Carnot process or negative temperature coefficient thermistors. In the nonlinear regime, dissipative structures are encountered even in the everyday world, for instance, in the form of heat convection of a candle light, cyclons, the famous Belousov–Zhabotinsky reaction[15] and, above all, in living organisms. The recently introduced new class of non-Hermitian systems, the so-called $\mathcal{PT}$-symmetric systems[16], have received considerable attention. In particular, optical structures provide an exceptional platform for the implementation of $\mathcal{PT}$-symmetric physics, where the (symmetric) refractive index distribution represents the real part of the complex potential, whereas the (antisymmetric) gain-loss profile has the role of its imaginary part[17]. In optical $\mathcal{PT}$-symmetrical systems, the short-term evolution of (optical) wave packets exhibits peculiar features and is highly non-intuitive[18–23]. In this context, perhaps, it is natural to ask how periodic but dissipative structures affect the long-term wave transport—a question of fundamental importance in numerous physical systems.

In this work, we theoretically predict and experimentally observe that in static $\mathcal{PT}$-symmetric lattice systems with no disorder, wave transport may suddenly slow down from ballistic to diffusive after a particular transition time. We find that this transition as well as the resulting diffusive transport—which, in the absence of disorder, is impossible in Hermitian systems—depends only on a dissipation parameter associated with the system. We verify our predictions by experiments in an optical waveguide array. In this paraxial optical setting, light propagating inside the waveguide array exhibits evolution analogous to that of a particle in a quantum mechanical lattice. Importantly, this system allows the direct observation of wave packets, which is a key to unravel the mechanism of the underlying transport.

Results

Theory. Let us first describe the theoretical basics of the transition from ballistic to diffusive transport in dissipative lattices. For illustration purposes, we employ a tight-binding model to describe the evolution of a wave packet in a biatomic lattice[24].

$$-i\frac{d}{dz}a_n(z) = [\delta_a + i\gamma_a]a_n(z) + \kappa(b_{n-1} + b_n)$$
$$-i\frac{d}{dz}b_n(z) = [\delta_b + i\gamma_b]b_n(z) + \kappa(a_{n+1} + a_n) , \quad (1)$$

where z is the evolution coordinate. The quantities $a_n(z)$, $b_n(z)$ are the propagating amplitudes in both lattice sites in unit cell n, the quantities δ_a and δ_b represent the real part of the potential, and γ_a

and γ_b represent the imaginary part of the potential (or gain/loss parameter), respectively. The transverse dynamics in the lattice is described by the hopping parameter (or coupling constant) κ. In the particular case of $\delta_a = \delta_b = \delta$ and $\gamma_a = -\gamma_b = \gamma$, the system is $\mathcal{PT}$-symmetric, as in this case the real part of the potential is symmetric and the imaginary part is antisymmetric[16,17]. A sketch of such a lattice is shown in Fig. 1a. In our analysis, however, we will not restrict ourselves to the $\mathcal{PT}$-symmetric case, but will consider a general non-Hermitian lattice with arbitrary $\delta_{a,b}$ and $\gamma_{a,b}$ instead. In this case, the evolution dynamics is dictated by the spectrum of propagation constants β:

$$\beta = \bar{\beta} \pm \sqrt{\left(\tilde{\delta} - i\tilde{\gamma}\right)^2 + 4\kappa^2\cos^2\left(\frac{q}{2}\right)} , \quad (2)$$

where q is the transverse Bloch momentum, $\bar{\beta} = (\delta_a + \delta_b)/2 + i(\gamma_a + \gamma_b)/2$, $\tilde{\delta} = (\delta_a - \delta_b)/2$, and $\tilde{\gamma} = (\gamma_b - \gamma_a)/2$. It is noteworthy that such a class of dissipative non-Hermitian systems is said to possess broken $\mathcal{PT}$-symmetry, as the eigenvalue spectrum is complex. Unbroken $\mathcal{PT}$-symmetry, that is, a purely real eigenvalue spectrum, can be achieved only in lattices with $\delta_a = \delta_b$ and an inhomogeneous inter-site coupling[25,26].

In Fig. 1b, an example of the spectrum (equation (2)) is shown. For this arrangement, the (normalized) lattice parameters are chosen to be $\delta_a = \gamma_a = 0\,\mathrm{cm}^{-1}$, $\delta_b = \gamma_b = 1\,\mathrm{cm}^{-1}$ and $\kappa = 1.5\,\mathrm{cm}^{-1}$. In this figure, the solid lines indicate the upper band (the '+' sign in equation (2)) and the dashed lines indicate the lower band (the '−' sign). Moreover, the blue lines represent the real part of the spectrum and the red lines the imaginary part. Clearly, the imaginary part of the eigenmode's propagation constant is a function of the transverse momentum q. Hence, eigenmodes in different regions of the spectrum will experience different losses, depending on the value of the imaginary part of their propagation constant. As a consequence, in both bands modes in the centre of the spectrum (where the lattice momentum $q \approx 0$) experience an intermediate loss, which is close to the average loss in the system. At the edge of the spectrum (around $q = \pm\pi$) the situation is very different. There, the modes in the upper band suffer from a loss that is much higher than the systems's average loss, whereas in the lower band the modes

a

b
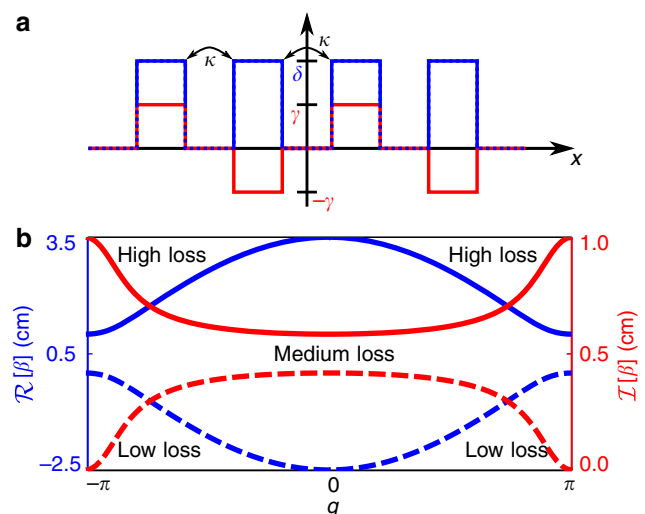
Figure 1 | $\mathcal{PT}$-symmetric lattice. (**a**) Sketch of the transverse profile of a biatomic $\mathcal{PT}$-symmetric lattice, where δ is the real part and γ is the imaginary part of the potential. The lattice sites are coupled with the strength κ. (**b**) The eigenvalue spectrum as a function of the lattice momentum q. Here the parameters $\delta_a = \gamma_a = 0\,\mathrm{cm}^{-1}$, $\delta_b = \gamma_b = 1\,\mathrm{cm}^{-1}$ and $\kappa = 1.5\,\mathrm{cm}^{-1}$ were assumed.

experience much less loss. Hence, because of decay, the modes in the upper band at the edge of the spectrum will disappear after a relatively short propagation distance z, whereas the modes in the centre of the spectrum will disappear somewhat later. Only the modes in the lower band around $q = \pm\pi$ will prevail at long propagation distances. Therefore, the spectrum will considerably be getting narrower during propagation of the wave packet along z, and only a part of the spectrum will contribute to transport.

To explore the impact of this phenomenon, we perform a numerical analysis. To this end, we solve the tight-binding equation (1) for an array of $N = 200$ waveguides using a standard Runge–Kutta scheme and calculate the variance $\sigma^2(z)$ at every computation step. A simulation of the wave evolution in a $\mathcal{PT}$-symmetric dissipative lattice is shown in Fig. 2a, where $\delta_a = \delta_b = \gamma_a = 0\,\mathrm{cm}^{-1}$, $\gamma_b = 2.0\,\mathrm{cm}^{-1}$ and $\kappa = 0.5\,\mathrm{cm}^{-1}$. Initially, the wave exhibits ballistic spreading as all eigenmodes still contribute to the transverse transport. However, after a certain propagation distance z the spreading clearly slows down, and the strongly modulated pattern, which is typical of ballistic transport in a periodic lattice, washes out completely. In Fig. 2b, a double-logarithmic plot shows the variance $\sigma^2(z)$ as a function of the gain/loss parameter γ_b. It is noteworthy that in the ballistic case, one finds $\sigma^2(z) \sim z^2$; plotting this with double-logarithmic axes results in a straight line with slope 2. In contrast, diffusive transport is characterized by $\sigma^2(z) \sim z^2$, which yields a straight line with slope 1 in a such a plot. Whereas one finds for $\gamma_a = \gamma_b = 0\,\mathrm{cm}^{-1}$ the expected ballistic spreading, for $\gamma_b > 0\,\mathrm{cm}^{-1}$ one clearly sees a sudden transition in the transport properties from initially ballistic (slope 2) to diffusive (slope 1). The distance, where this transition happens decreases as the loss parameter γ_b increases (note that $\gamma_a = 0\,\mathrm{cm}^{-1}$ for all graphs). We attribute this phenomenon to the narrowing of the spectrum: after some

specific propagation distance z_{crit}, essentially only a part of the spectrum contributes to transport. In fact, the continuous spectral contraction leads to the characteristic diffusive spread of the wave packet observed in our simulations.

To understand this process beyond the intuitive spectrum-based explanation of this effect, we developed a full analytical theory of this effect, which is provided in the Methods section. Within this theory, the critical distance around which transport slows down from ballistic to diffusive is given by

$$z_{\mathrm{crit}} \approx \frac{2}{\tilde{\gamma}}. \qquad (3)$$

Around z_{crit}, the spectral narrowing reaches a strength that impedes ballistic transport because of an insufficient number of propagating modes. Therefore, in essence for $z \ll z_{\mathrm{crit}}$ the transport is ballistic, whereas for $z \gg z_{\mathrm{crit}}$ it enters the diffusive regime. Importantly, the critical distance z_{crit} depends strongly on the difference in the loss parameters $\tilde{\gamma}$, and the dependence on the coupling coefficients κ is negligible. Interestingly, our simulations also indicate that z_{crit} slightly shifts to larger values for $|\tilde{\delta}| > 0\,\mathrm{cm}^{-1}$.

Experiment. For the experimental demonstration of our theoretical results, we fabricated various optical waveguide samples employing the direct-laser writing technology[27]. A sketch of such a waveguide array is shown in Fig. 3a, and a microscopic image from the end facet of one specific realization is shown in Fig. 3b. For further details of the fabrication process, we refer the reader to the Methods section. Each sample was 10 cm long and contains 60 waveguides with an inter-site spacing of $d = 17\,\mu\mathrm{m}$. These parameters were chosen such that the light does not reach the boundaries of the lattice during propagation.

To introduce additional, well-defined losses in every second guide, these sites are sinusoidally modulated transverse to the lattice plane with an amplitude of $A = 3\,\mu\mathrm{m}$. The induced curvature then facilitates radiation and, therefore, enhanced losses. These losses can be tuned precisely by changing the curvature of the waveguide modulation, which we achieve by adjusting the period of the modulation at constant amplitude. In our study, depending on the specific sample, the number of periods per sample length was ranging between 23 and 103. Note that for such small modulation amplitudes of only $A = 3\,\mu\mathrm{m}$, the
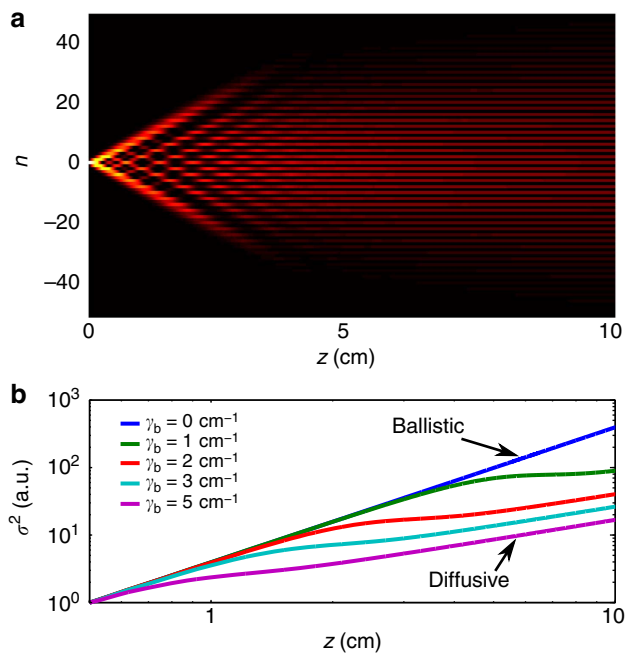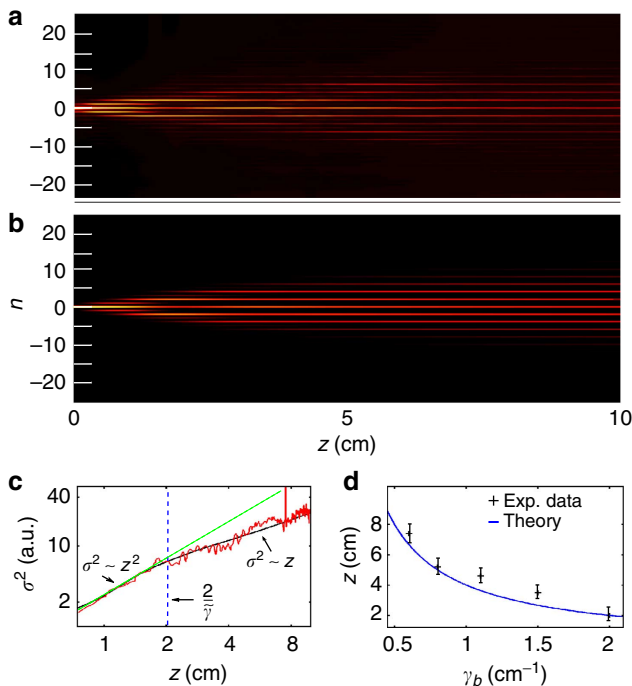

Figure 2 | Wave evolution in dissipative $\mathcal{PT}$-symmetric lattices. (**a**) Simulation of the wave evolution in a quasi $\mathcal{PT}$-symmetric system with $\delta_a = \delta_b = \gamma_a = 0\,\mathrm{cm}^{-1}$, $\gamma_b = 2.0\,\mathrm{cm}^{-1}$ and $\kappa = 0.5\,\mathrm{cm}^{-1}$. In the beginning, the transport shows clear signatures of ballistic spreading, whereas for larger propagation distances the evolution is diffusive. (**b**) The calculated variance of the evolving wave packet as a function of the distance z and the gain/loss parameter γ_b. All other parameters are kept constant so that the red curve corresponds to **a**.
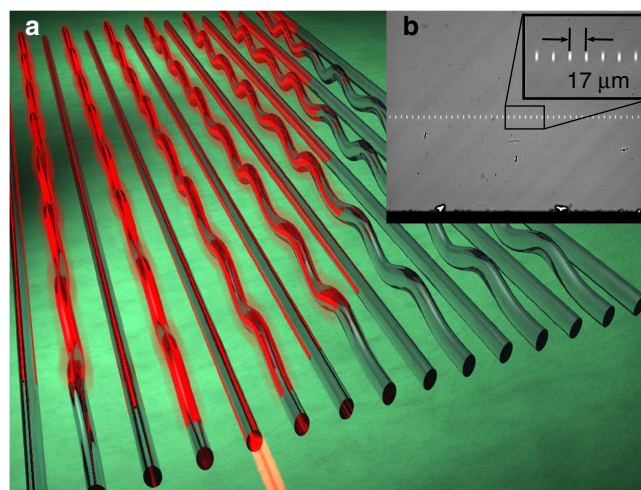
Figure 3 | Experimental realization of dissipative $\mathcal{PT}$-symmetric lattices. (**a**) Sketch of the fabricated waveguide arrays, where every second waveguide is sinusoidally modulated to obtain strong and controllable radiation losses. (**b**) Microscope image from the front facet of a sample.

average spacing between the waveguides is always $d \approx 17\,\mu m$, resulting in a homogeneous coupling constant κ. However, the modulation causes a slight rise of the propagation constant in the modulated guides because of the increased optical path. This can be compensated by artificially increasing the refractive index of the unmodulated waveguides. However, the mobility transition in non-Hermitian lattices takes place also for $|\tilde{\delta} > 0|$; hence, in our samples we did not compensate for the additional detuning of the modulated guides.

Our experimental results are summarized in Fig. 4. To excite the entire spectrum, we launch light into the central waveguide of the lattice. An image of the propagating light beam is shown in Fig. 4a, obtained using a fluorescence microscopy technique[28] (see Methods section). For small propagation distances, the typical ballistic diffraction pattern is observed, whereas for larger propagation distances the modulation of the pattern washes out and the spreading slows down. In Fig. 4b, we show a simulation of the experimental pattern with parameters $\delta_a = \delta_b = \gamma_a = 0\,cm^{-1}$, $\gamma_b = 2\,cm^{-1}$ and $\kappa = 1.1\,cm^{-1}$. From the experimental fluorescence microscopy pattern in Fig. 4a, we extract the variance, which we plot using a double-logarithmic plot in Fig. 4c. The transition from ballistic to diffusive transport is clearly visible at $z_{crit} \approx 2\,cm$: the initial ballistic spread (slope 2) suddenly slows down to diffusive (slope 1). We would like to emphasize the remarkable agreement between both the experimental and theoretical curve, as for the simulation no fitting

parameters were used. The coupling parameter $\kappa = 1.1\,cm^{-1}$ used in the simulation is an experimental value obtained from measurements in a single directional coupler with a waveguides separation of $17\,\mu m$. The loss parameter $\gamma_b = 2\,cm^{-1}$ was extracted from loss measurements in isolated sinusoidally bent waveguides.

We repeat our experiments for different modulation periods in the waveguides, which results in different loss parameters γ_b. The position of the transition point z_{crit} is extracted from the fluorescence images and is plotted in Fig. 4d. As predicted by our theory, the value of z_{crit} is in very good agreement with equation (3). The fluorescence images and variance plots of all data points in Fig. 4a are shown in Fig. 5.

Discussion

For the first time, we have observed the coexistence of ballistic and diffusive transport in a static, ordered system, based on non-Hermiticity. The inhomogeneous losses associated with the eigenmodes result in a contraction of the spectrum, which hinders ballistic transport because of an insufficient number of propagating modes. The transition from the initially ballistic motion to a diffusive transport is generally impossible in static Hermitian systems, where sub-ballistic transport is only possible through the introduction of disorder. Moreover, it was shown that the critical distance—where the transition of the transport regimes takes place—depends only on the degree of dissipation and not on the coupling between the waveguides.

Our theoretical and experimental work suggests various intriguing questions. In terms of applications, can a non-Hermitian waveguide lattice be used as a sophisticated mode filtering device, for any desired Bloch waves and not only those at the edge of the Brillouin zone (around $q = \pi$)? Can one design a device with real-time loss control to actively tune the width of the beam at the sample's output facet? These issues might be of particular interest in the fields of telecommunication or quantum computing, as especially in the field of quantum optics there is a great desire to prepare single as well as entangled photons in well-defined states. Moreover, also from the more fundamental side, many interesting questions arise: what is the impact of losses in two-dimensional systems, in particular photonic graphene[29]? How the light behaves at defects and interfaces in lossy systems? Does disorder or nonlinearitiy facilitate or hinder transport[30]? Moreover, can the band structure be modified via higher-order coupling effects[31] to achieve different transport regimes such as sub-diffusive, super-diffusive or even super-ballistic transport[32]? Our work will enable these questions, as well as many others, to be addressed.

Figure 4 | Experimental results. (a) Fluorescence microscopy image of the light beam as propagating through the lattice. (b) Simulation resulting in a similar propagation pattern as in a. The simulation parameters were the same as in the experiment, namely, $\delta_a = \delta_b = \gamma_a = 0\,cm^{-1}$, $\gamma_b = 2\,cm^{-1}$ and $\kappa = 1.1\,cm^{-1}$. (c) The variance of the experimental (a) and simulated (b) beam in a double-log plot as a function of the propagation distance z (red line, experimental data; black line, simulation). The transition from ballistic transport (slope 2) to diffusive transport (slope 1) is clearly visible. The green dashed line acts as a guide for the eye, to illustrate a continued ballistic transport. (d) The transition point z_{crit} as a function of the loss parameter γ_b extracted from various samples (black crosses). The error bars represent a 95% confidence interval. The data show a clear correspondence to the theoretically predicted reciprocal dependency (blue line).

Methods

Theoretical foundation. To derive the corresponding results, we start from the following system of equations:

$$-i\partial_z a_n = [\delta_a + i\gamma_a]a_n + \kappa b_{n-1} + c b_n$$
$$-i\partial_z b_n = [\delta_b + i\gamma_b]b_n + \kappa b_{n+1} + c a_n. \tag{4}$$

The first step in analysing this system is extracting its eigenvalue spectrum. This is done by starting with the usual ansatz
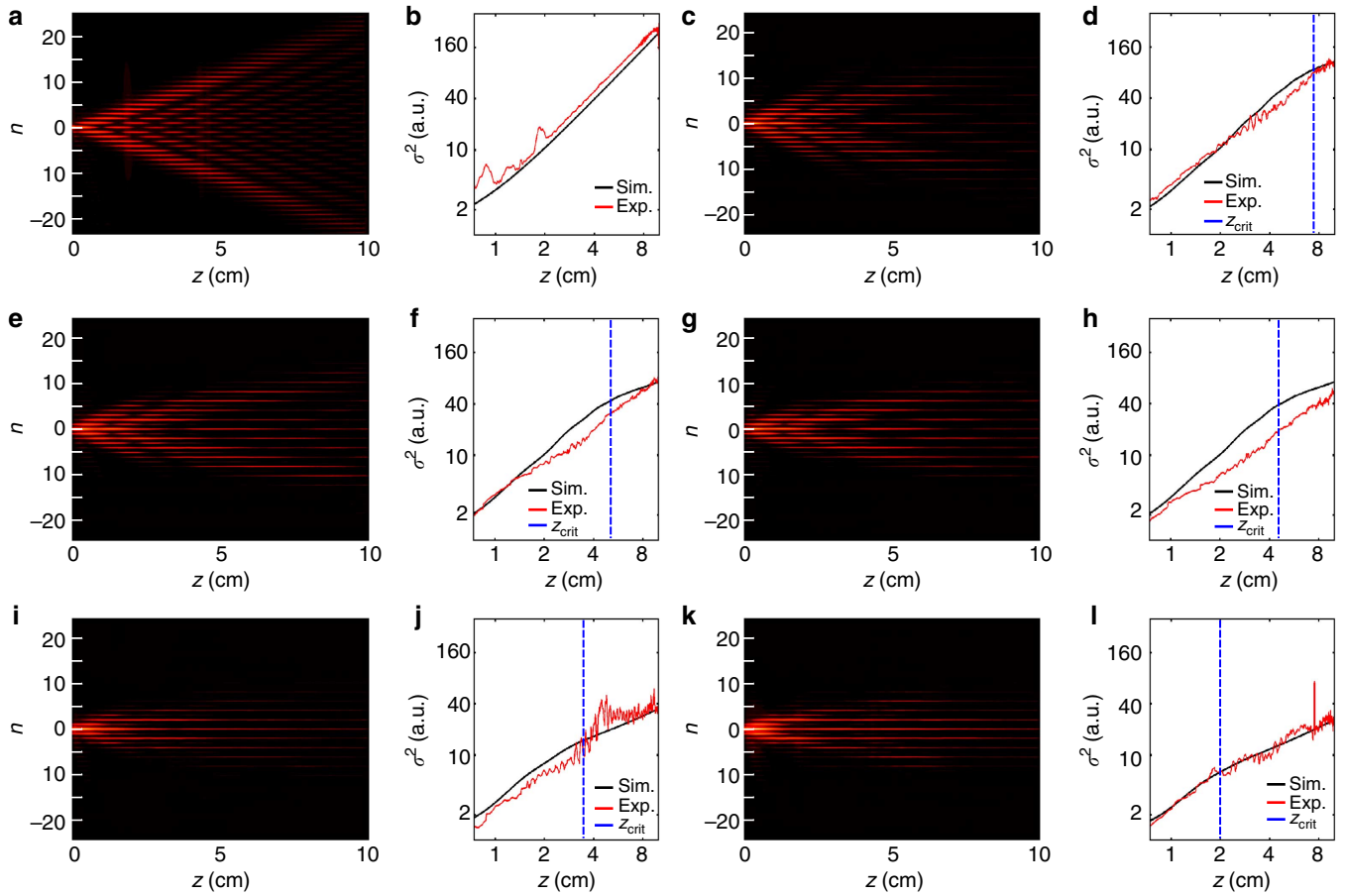
$$\begin{pmatrix} a_n \\ b_n \end{pmatrix}(q) = e^{i\beta(q)z}e^{inq}\begin{pmatrix} a_0 \\ b_0 \end{pmatrix}_q. \tag{5}$$

Substituting this into equation (4), one arrives at an expression that determines the eigenvalues $\beta(q)$ as well as the eigenvectors $(a_0\, b_0)_q^T$:

$$\beta\begin{pmatrix} a_n \\ b_n \end{pmatrix} = \begin{pmatrix} \delta_a + i\gamma_a & \kappa e^{-iq} + c \\ \kappa e^{iq} + c & \delta_b + i\gamma_b \end{pmatrix}\begin{pmatrix} a_n \\ b_n \end{pmatrix}. \tag{6}$$

Therefore, the eigenvalue spectrum is given by

$$\beta_\pm = \bar{\beta} \pm \sqrt{\left(\tilde{\delta} - i\tilde{\gamma}\right)^2 + \kappa^2 + c^2 + 2\kappa c \cos q}, \tag{7}$$

Figure 5 | Experimental data. Subfigures **a**, **c**, **e**, **g**, **i** and **k** show fluorescence microscopy images of the light beams propagating through the lattice. Subfigures **b**, **d**, **f**, **h**, **j** and **l** contain the corresponding variance in a double-log plot as a function of the propagation distance z. The experimental data are given by the red line, whereas the black line depicts the corresponding simulation. The vertical dashed blue line illustrates the experimentally observed transition distance z_{crit}. **a** and **b** show the purely ballistic case with $\gamma_b = 0$. In **c** and **d**, $\gamma_b = -0.6 \, cm^{-1}$; **e** and **f** $\gamma_b = -0.8 \, cm^{-1}$; (**g** and **h**) $\gamma_b = -1.1 \, cm^{-1}$; (**i** and **j**) $\gamma_b = -1.5 \, cm^{-1}$; (**k** and **l**) $\gamma_b = -2 \, cm^{-1}$.

where

$$\bar{\beta} = \frac{\delta_a + \delta_b + i(\gamma_a + \gamma_b)}{2}$$
$$\bar{\delta} = \frac{\delta_a - \delta_b}{2}$$
$$\bar{\gamma} = \frac{\gamma_b - \gamma_a}{2}$$
.

The corresponding eigenvectors are

$$\begin{pmatrix} a_0 \\ b_0 \end{pmatrix}_{q,\pm} = \begin{pmatrix} \frac{\beta_{\pm} - \bar{\beta} + \bar{\delta} - i\bar{\gamma}}{\kappa e^{iq} + c} \\ 1 \end{pmatrix}. \qquad (8)$$

As described in the paper, we are interested in the evolution of a single waveguide excitation. For this specific case, the initial conditions (at $z = 0$) are $a_n = \delta_{n0}$ and $b_n = 0$. From these initial conditions, it is straight forward to write down the evolution of the wave packet in the form of an integral:

$$\begin{pmatrix} a_n \\ b_n \end{pmatrix}(z) = \frac{1}{2\pi} \int_0^{2\pi} \frac{\kappa e^{iq} + c}{\beta_+ - \beta_-} \left[\begin{pmatrix} \frac{\beta_+ - \bar{\beta} + \bar{\delta} - i\bar{\gamma}}{\kappa e^{iq} + c} \\ 1 \end{pmatrix} e^{i\beta_+ z} - \begin{pmatrix} \frac{\beta_- - \bar{\beta} + \bar{\delta} - i\bar{\gamma}}{\kappa e^{iq} + c} \\ 1 \end{pmatrix} e^{i\beta_- z} \right] e^{inq} dq. \quad (9)$$

Equation (9) is the full formal solution of equation (4) with the given initial conditions. However, given this form of solution it is difficult to predict a transition from ballistic to diffusive transport. On this account, the goal of this section is to derive the existence of such a transition.

As discussed in the main text, the transport regime is solely determined by the variance of the wave packet. Consequently, we calculate the variance of the wave packet given by equation (9) for large propagation distances z. For simplicity, in the following we will only consider the variance on the a_n sublattice. However, the derivation for the b_n sublattice follows analogously to the way presented.

For simplicity, let us assume that the b_n waveguides exhibit more loss than the a_n waveguides, that is, $\gamma_b > \gamma_a$. From this it follows that $\bar{\gamma}$ is a positive quantity. Keeping this in mind, let us take yet another look at the eigenvalue spectrum

(equation (7)). It was already stated in the main text that the specific case of $\kappa = c$ always leads to a complex spectrum. From here on, let us proceed with this specific case. For such a complex spectrum, the modes that exhibit the least amount of loss are those in the lower band ($\beta - q$) around $q \approx \pi$. Hence, for large propagation distances z, one can approximate the evolution of the a_n by

$$a_n(z) = \frac{1}{2\pi} e^{i(\bar{\beta} + \bar{\delta} - i\bar{\gamma})z} e^{in\pi} \int_{-\infty}^{\infty} e^{-wq'^2 z} e^{inq'} dq'. \qquad (10)$$

To arrive at this point, first we have neglected the contribution of the modes of the upper band. Second, we have used the Taylor expansion of $\beta_{\pm}$ around $q = \pi$, which reads

$$\beta_{\pm} = \bar{\beta} \mp \left(\bar{\delta} - i\bar{\gamma} \right) \mp \frac{\kappa^2 \left(\bar{\delta} + i\bar{\gamma} \right)}{2 \left(\bar{\delta}^2 + \bar{\gamma}^2 \right)} (q - \pi)^2. \qquad (11)$$

Because of the dominance of the Gaussian term $e^{-wq^2 z}$, for large z one can approximate

$$\frac{\beta_- - \bar{\beta} + \bar{\delta} - i\bar{\gamma}}{\beta_+ - \beta_-} \xrightarrow{z \to \infty} -1. \qquad (12)$$

In equation (10), also $q' = q + \pi$ and

$$w = \frac{\kappa^2 \left(\bar{\gamma} - i\bar{\delta} \right)}{2 \left(\bar{\delta}^2 + \bar{\gamma}^2 \right)} \qquad (13)$$

have been used. The extension of the integration limits in equation (10) can be justified because of the fact that for large z, the width of the Gaussian is much smaller than the initial integration range. At this point, it needs to be emphasized that the approximation performed in equation (7) is only valid for a non-vanishing

real part of w. Moreover, this condition is equivalent to the demand of a non-vanishing loss detuning.

Finally, the evaluation of the integral in equation (10) yields

$$a_n(z) = \frac{1}{2\sqrt{\pi w z}} e^{i(\bar{\beta} + (\tilde{\delta} - i\tilde{\gamma}))z} e^{in\pi} e^{-\frac{n^2}{4wz}}. \tag{14}$$

Now, the last step in the analysis will be to calculate the variance of the wave packet. The variance for such a discrete and dissipative system is defined by

$$\sigma^2 = \frac{\sum_{n=0}^{\infty} n^2 |a|^2}{\sum_{n=0}^{\infty} |a|^2}. \tag{15}$$

Using the explicit form of a_n, one obtains

$$\sigma^2 = \frac{\sum_{n=0}^{\infty} n^2 e^{-\frac{\Re[w]n^2}{2|w|^2 z}}}{\sum_{n=0}^{\infty} e^{-\frac{\Re[w]n^2}{2|w|^2 z}}}. \tag{16}$$

For large z, the sums can be approximated by integrals using $x = n/\sqrt{z}$ and $\Delta x \xrightarrow{z \to \infty} 0$. Hence, one finds

$$\sigma^2 = z \frac{\int_0^{\infty} x^2 e^{-\frac{\Re[w]x^2}{2|w|^2}} dx}{\int_0^{\infty} e^{-\frac{\Re[w]x^2}{2|w|^2}} dx}. \tag{17}$$

Evaluating the Gaussian integral yet again, one finds the variance to be

$$\sigma^2 = \frac{|w|^2}{\Re[w]} z = \frac{\kappa^2}{2\tilde{\gamma}} z. \tag{18}$$

This shows mathematically that the variance rises with the first power of z. Hence, the propagation of the wave packet is diffusive.

Subsequently, we want to derive the approximate region of the transition, which corresponds to the critical distance z_{crit} given by equation (3). For simplicity, we only regard the case of $\tilde{\delta} = 0$. For the approximation (equation (10)) to hold, all modes outside an ε-region around $q = \pi$ need to be damped sufficiently, and hence need to be smaller than some value δ. For our analysis, it is sufficient to fix δ at $\delta = e^{-2}$. This damping condition reads

$$e^{-\Re[w]\varepsilon^2 z} < \delta, \tag{19}$$

or equivalently

$$z > \frac{4\tilde{\gamma}}{\varepsilon^2 \kappa^2}. \tag{20}$$

It is important to note that ε cannot be chosen arbitrarily, but one has the additional condition

$$\tilde{\gamma} > \frac{\kappa^2}{2\tilde{\gamma}} \varepsilon^2, \tag{21}$$

which follows from the evaluation of the denominator in equation (12) and the Taylor expansion of the eigenvalues. Connecting both conditions, one obtains equation (3).

Waveguide fabrication. Our samples are fabricated in bulk-fused silica wafers using the femtosecond laser direct-write aproach[27] employing a Ti:Sapphire Mira/RegA laser system (Coherent Inc.) operating at a wavelength of 800 nm, a repetition rate of 100 kHz and a pulse length of 170 fs. The light is focused inside the sample by a $\times 20$ microscope objective (NA $= 0.35$), and by continuously moving the sample using a high-precision positioning system (Aerotech Inc.) the waveguides are created by the induced refractive index increase. For the fabrication of our samples, the pulse energy was adjusted to 320 nJ and the writing velocity was set to 1.5 mm s^{-1}.

To introduce enhanced and controllable losses to specific waveguides, an additional sinusoidal modulation was applied to the waveguides to achieve additional radiation losses. The modulation is introduced into the vertical direction, as this prevents the radiated light from travelling through the lattice and being recollected by other waveguides.

Fluorescence microscopy. For the direct monitoring of the light propagation in our samples (see Fig. 4a), we used a fluorescence microscopy technique[28]. A massive formation of non-bridging oxygen hole colour centres occurs during the writing process, when fused silica with a high content of hydroxide is used, resulting in a homogeneous distribution of these colour centers along the waveguides. When light from a Helium-Neon laser at $\lambda = 633$ nm is launched into the waveguides, the non-bridging oxygen hole colour centres are excited and the resulting fluorescence ($\lambda = 650$ nm) can be directly observed using a charge-coupled device camera with an appropriate narrow linewidth filter. As the colour centres are formed exclusively inside the waveguides, this technique yields a high signal-to-noise ratio.

References

1. Drude, P. Zur elektronentheorie der metalle. *Ann. Phys.* **306,** 566–613 (1900).
2. Kittel, C. & Kroemer, H. *Thermal Physics* (WH Freeman, 1980).
3. Ottino, J. M. & Wiggins, S. Introduction: mixing in microfluidics. *Philos. Trans. Roy. Soc. Lond. Ser. A: Math. Phys. Eng. Sci.* **362,** 923–935 (2004).
4. Stejskal, E. O. & Tanner, J. E. Spin diffusion measurements: spin echoes in the presence of a time-dependent field gradient. *J. Chem. Phys.* **42,** 288–292 (1965).
5. Schwartz, T., Bartal, G., Fishman, S. & Segev, M. Transport and anderson localization in disordered two-dimensional photonic lattices. *Nature* **446,** 52–55 (2007).
6. Rittner, A. S. C. & Reppy, J. D. Disorder and the supersolid state of solid ^{4}He. *Phys. Rev. Lett.* **98,** 175302 (2007).
7. Holt, R. G., Clarke, C. C. & McDaniel, J. G. An acoustic levitation technique for measuring the rheology of foam near the order-disorder transition. *J. Acoust. Soc. Am.* **105,** 1146–1146 (1999).
8. Billy, J. *et al.* Direct observation of anderson localization of matter waves in a controlled disorder. *Nature* **453,** 891–894 (2008).
9. Roati, G. *et al.* Anderson localization of a non-interacting bose-einstein condensate. *Nature* **453,** 895–898 (2008).
10. Anderson, P. W. Absence of diffusion in certain random lattices. *Phys. Rev.* **109,** 1492–1505 (1958).
11. Lahini, Y. *et al.* Anderson localization and nonlinearity in one-dimensional disordered photonic lattices. *Phys. Rev. Lett.* **100,** 013906 (2008).
12. Amir, A., Lahini, Y. & Perets, H. B. Classical diffusion of a quantum particle in a noisy environment. *Phys. Rev. E* **79,** 050105 (2009).
13. Barthelemy, P., Bertolotti, J. & Wiersma, D. S. A lévy flight for light. *Nature* **453,** 495–498 (2008).
14. Marksteiner, S., Ellinger, K. & Zoller, P. Anomalous diffusion and lévy walks in optical lattices. *Phys. Rev. A* **53,** 3409–3430 (1996).
15. Glansdorff, P. & Prigogine, I. *Thermodynamic Theory of Structure, Stability and Fluctuations* (John Wiley & Sons Ltd, 1971).
16. Bender, C. M. & Boettcher, S. Real spectra in non-hermitian hamiltonians having PT symmetry. *Phys. Rev. Lett.* **80,** 5243–5246 (1998).
17. El-Ganainy, R., Makris, K. G., Christodoulides, D. N. & Musslimani, Z. H. Theory of coupled optical -symmetric structures. *Opt. Lett.* **32,** 2632–2634 (2007).
18. Makris, K. G., El-Ganainy, R., Christodoulides, D. N. & Musslimani, Z. H. Beam dynamics in PT symmetric optical lattices. *Phys. Rev. Lett.* **100,** 103904 (2008).
19. Musslimani, Z. H., Makris, K. G., El-Ganainy, R. & Christodoulides, D. N. Optical solitons in PT periodic potentials. *Phys. Rev. Lett.* **100,** 030402 (2008).
20. Longhi, S. Bloch oscillations in complex crystals with symmetry. *Phys. Rev. Lett.* **103,** 123601 (2009).
21. Guo, A. *et al.* Observation of PT-symmetry breaking in complex optical potentials. *Phys. Rev. Lett.* **103,** 093902 (2009).
22. Rüter, C. E. *et al.* Observation of parity-time symmetry in optics. *Nat. Phys.* **6,** 192–195 (2010).
23. Regensburger, A. *et al.* Parity-time synthetic photonic lattices. *Nature* **488,** 167–171 (2012).
24. Yariv, A. *Optical Electronics* 4th edn (Saunders College Publishing, 1991).
25. Zheng, M. C., Christodoulides, D. N., Fleischmann, R. & Kottos, T. PT optical lattices and universality in beam dynamics. *Phys. Rev. A* **82,** 010103 (2010).
26. Dmitriev, S. V., Sukhorukov, A. A. & Kivshar, Y. S. Binary parity-time-symmetric nonlinear lattices with balanced gain and loss. *Opt. Lett.* **35,** 2976–2978 (2010).
27. Szameit, A. & Nolte, S. Discrete optics in femtosecond-laser-written photonic structures. *J. Phys. B* **43,** 163001 (2010).
28. Szameit, A. *et al.* Quasi-incoherent propagation in waveguide arrays. *Appl. Phys. Lett.* **90,** 241113 (2007).
29. Szameit, A., Rechtsman, M. C., Bahat-Treidel, O. & Segev, M. -symmetry in honeycomb photonic lattices. *Phys. Rev. A* **84,** 021806 (2011).
30. Jovic, D. M., Denz, C. & Belic, M. R. Anderson localization of light in -symmetric optical lattices. *Opt. Lett.* **37,** 4455–4457 (2012).
31. Szameit, A. *et al.* Long-range interaction in waveguide lattices. *Phys. Rev. A* **77,** 043804 (2008).
32. Levi, L., Krivolapov, Y., Fishman, S. & Segev, M. Hyper-transport of light and stochastic acceleration by evolving disorder. *Nat. Phys.* **8,** 912–917 (2012).

Author contributions

T.E. and A.S. developed the theory. T.E. and R.H. performed the simulations. T.E. and F.D. carried out the experimental work. A.S. supervised the project. All authors co-wrote the paper.

Additional information

Competing financial interests: The authors declare no competing financial interests.

7